

A 2 day orbital period for a redback millisecond pulsar candidate in the globular cluster NGC 6397

Manuel Pichardo Marcano¹, *L.E. Rivera Sandoval^{1,2}, Thomas J. Maccarone¹, Yue Zhao²,
Craig O. Heinke²

¹*Department of Physics and Astronomy, Texas Tech University, Lubbock, TX 79409*

²*Department of Physics, University of Alberta, CCIS 4-183, Edmonton, AB, T6G 2E1, Canada*

ABSTRACT

We report optical modulation of the companion to the X-ray source U18 in the globular cluster NGC 6397. U18, with combined evidence from radio and X-ray measurements, is a strong candidate as the second redback in this cluster, initially missed in pulsar searches. This object is a bright variable star with an anomalous red color and optical variability (~ 0.2 mag in amplitude) with a periodicity ~ 1.96 days that can be interpreted as the orbital period. This value corresponds to the longest orbital period for known redback candidates and confirmed systems in Galactic globular clusters and one of the few with a period longer than 1 day.

Key words: globular clusters: general; globular clusters: individual (NGC 6397); X-rays: binaries pulsars

1 INTRODUCTION

Redback pulsars are a sub-type of binary millisecond pulsars (MSPs) with main sequence, or slightly evolved, low mass companions ($M_c \approx 0.2 - 0.9M_\odot$) (Roberts 2013). They differ from the closely related black widows by having companions which are non-degenerate, and a bit more massive, than the $\lesssim 0.1M_\odot$ degenerate companions in the black widow systems. Both classes are characterized by radio eclipses due to excess ionized gas within the system, which suggests that the companion is being ablated by irradiation from the pulsar wind (Fruchter et al. 1988a,b). These systems are important for understanding the evolution of MSPs as their formation mechanisms and eventual fates are open questions.

Chen et al. (2013) and Benvenuto et al. (2014) propose contrasting views about the evolutionary tracks leading to the formation of a redback system, and whether or not these end as black widows. Chen et al. (2013) concluded that redbacks and black widow pulsars follow different evolutionary paths depending on the strength of evaporation, finding that black widows do not descend from redback pulsars, while Benvenuto et al. (2014) concluded that black widows can descend from redbacks, depending on the evaporation and irradiation feedback on the system.

Other open questions remain regarding redbacks and their relation with transitional MSPs (tMSPs).¹ A handful of redbacks are confirmed tMSPs (PSR J1023+0038, PSR J1824-2452I, and PSR J1227-4853; Archibald et al. 2009; Papitto et al. 2013; Bassa et al. 2014). It is not clear if all redbacks will eventually show transitional

behaviour if observed over a long period of time, but long-term follow up of these systems is vital and can help guide the needed theoretical work on this topic.

Optical and X-ray observations can provide relevant information regarding the redback systems and help guide future radio searches. The X-ray spectra of redbacks consist of a dominant non-thermal component and at least one thermal component, likely originating from the heated pulsar polar caps (Zavlin et al. 1996, 2002; Bogdanov et al. 2005, 2011). The non-thermal emission from MSPs can be produced by two different mechanisms: coherent emission from the magnetosphere or non-thermal emission due to an intrabinary shock between the pulsar wind and the companion's material (Stappers et al. 2003). The latter has been shown to be important for the confirmed redback MSPs, as the non-thermal emission is orbitally modulated (Bogdanov et al. 2005, 2010, 2011). In the optical, redbacks show orbital modulation due to effects such as the ellipsoidal modulation of the near-Roche filling companion, and day vs night side temperature differentials due to heating of the secondary from the pulsar or intrabinary shocks (e.g. Callanan et al. 1995; Romani & Sanchez 2016; Cho et al. 2018). Modeling of their optical lightcurves has been done for a handful of these systems, to obtain constraints on the component masses and inclinations (Thorstensen & Armstrong 2005; Cho et al. 2018; Strader et al. 2019).

The known redbacks are also of special interest as they have higher average neutron star masses than the canonical mass of $\sim 1.4M_\odot$, with a median mass of $1.78 \pm 0.09M_\odot$ (Strader et al. 2019), with some having evidence of hosting neutron stars with masses larger than $2M_\odot$ (Linares 2018; Strader et al. 2019; Kandel & Romani 2020). Mapping out their populations and evolutionary tracks is thus important for understanding binary evolution. Unfortunately, these systems can be particularly hard to find in radio

* Contact e-mail: manuel.pichardo-marcano@ttu.edu

¹ tMSPs are accreting millisecond pulsars that switch between accreting X-ray binary and millisecond radio pulsar states.

pulsar searches as the pulses from the neutron star can be eclipsed, or scattered out, by the ionized stripped gas from the hydrogen rich companion star (e.g. Fruchter et al. 1988a). Currently there are 25 redbacks or redback candidates in the Galactic field (Strader et al. 2019; Swihart et al. 2020), and 13 confirmed redbacks in 8 globular clusters. These pulsar searches can be computationally demanding, especially for an unknown orbital period. Furthermore, the variation in the dispersion measure expected in the redback systems as the radio pulse propagates through the companion’s wind can add an additional computational parameter to the search.

NGC 6397 is the closest (2.4 kpc) core-collapsed globular cluster, with an average reddening of $E(B - V) = 0.18$ (Harris 1996; McLaughlin & van der Marel 2005). Due to its proximity and low reddening, NGC 6397 has been extensively studied at different wavelengths. Cool et al. (1993) first detected X-ray sources in NGC 6397, with the *ROSAT* satellite. Optical and UV observations with the *Hubble Space Telescope* (HST) have enabled the identification of several X-ray sources with blue, variable, and/or $H\alpha$ bright stars (Cool et al. 1995; Grindlay et al. 1995; Cool et al. 1998; Taylor et al. 2001; Ferraro et al. 2001; Shara et al. 2005). Identifications were dramatically improved by the sub-arcsecond positions of the *Chandra X-ray Observatory* (Grindlay et al. 2001; Bogdanov et al. 2010), enabling identification of many more optical/UV counterparts with HST (Kaluzny et al. 2006; Cohn et al. 2010; Heinke et al. 2014; Pallanca et al. 2017; Dieball et al. 2017). NGC 6397 has also been observed with radio telescopes, both imaging observations with the *Australia Telescope Compact Array* (ATCA) (Zhao et al. 2020), and radio pulsar searches with Parkes (D’Amico et al. 2001) that discovered PSR J1740-5340 (aka the X-ray source U12, Grindlay et al. 2001) and confirmed its nature as an eclipsing redback system.

Using ground-based data, Kaluzny et al. (2006) reported a 1.3 day periodicity for the source V31, which they associated with U18. Bogdanov et al. (2010) studied the X-ray properties of U18 and found similarities in its luminosity and spectrum with the confirmed MSP U12, as both sources have a dominant non-thermal component, possibly from an intrabinary shock. Bogdanov et al. (2010) did not find the claimed periodicity of 1.3 days reported by Kaluzny et al. (2006) in the X-ray data of U18, and dismissed V31 as the possible optical counterpart of U18 based on the distance between them (2.1σ) and the presence of a more likely optical counterpart closer to the X-ray source (Grindlay et al. 2001). Bogdanov et al. (2010) suggested U18 as a likely second MSP in the cluster, based on the similarity of its X-ray and optical properties to those of the MSP PSR J1740-5340. This interpretation of U18 as a redback was further strengthened by the radio detection of U18 with a steep spectrum, as typical of pulsars (Zhao et al. 2020).

U18 has also been observed twice with the Multi Unit Spectroscopic Explorer (MUSE Bacon et al. 2014). Husser et al. (2016) reported two observations 22 h apart, during MUSE commissioning in Summer 2014. In their full-spectrum fitting analysis they found a K subgiant with $\log g \approx 3.6$ and $T_{\text{eff}} \approx 4200\text{K}$ as the best fit for the optical counterpart of U18, and calculated a radial velocity difference between the two observations of $\Delta v_{\text{rad}} = 145.9 \text{ km s}^{-1}$.

Here we discover an orbital period of 1.96 ± 0.06 days for the strong redback candidate U18. As U18 is in one of the closest globular clusters, it is a perfect candidate for high resolution spectroscopic follow-up to fully characterize its orbit, adding to a small sample of redbacks with well constrained dynamically determined masses.

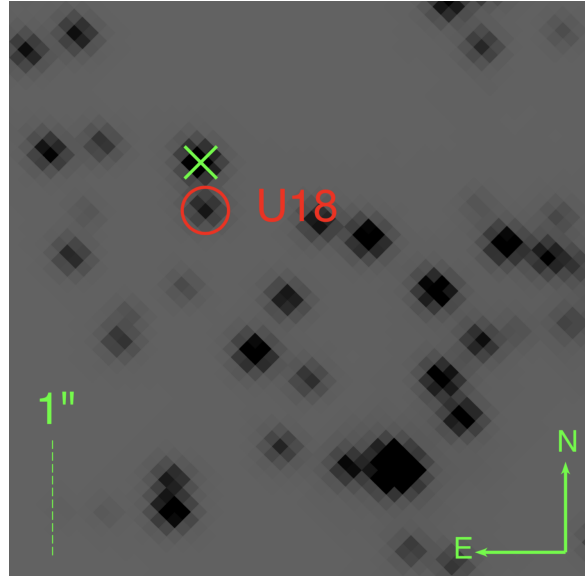


Figure 1. 5"×5" WFPC2 image around U18 in F336W. U18 is marked by the 0.2" radius red circle. V31 is the star north of U18 $\sim 0.4''$ away marked with an X. North is up and East is left.

2 DATA ANALYSIS AND REDUCTION

We use WFPC2 data from the parallel field of the HST large program GO-10424 (Richer et al. 2006), which covered the cluster center (the primary field, using the ACS camera, is arcminutes away). The data consist of 126 orbits, and each WFPC2 orbit is divided into three exposures, in the filters F814W, F606W and F336W. We use the F336W data to avoid crowding in the field, taking advantage both of the somewhat better diffraction limit in the bluer band, and the smaller number of bright stars in the bluer band given the globular cluster’s old stellar population. This results in 126 individual exposures (one exposure per orbit) in F336W with exposure times ranging from 500-700 seconds, taken between mid-March and early April 2005 (2005-13-03 to 2005-08-04). The minimum separation between data points being 74 minutes and the maximum of 3.2 days with a total baseline of 26 days.

For the photometry, we use DOLPHOT (Dolphin 2000) including the WFPC2 Module to perform point-spread-function photometry. We supply DOLPHOT the calibrated single-exposure image data (c0m) WFPC2 files and the drizzled .drz image as the reference frame for alignment. The final output from the software lists the position of each star relative to the reference image, together with the measured aperture-corrected magnitudes calibrated to the Vega system for the individual exposures, along with some diagnostic values. We limit the data to measurements containing an error flag of zero meaning that the star was recovered extremely well in the image without contamination due to cosmic rays.

From the DOLPHOT output, we construct a lightcurve for the optical counterpart of U18 (see Fig. 1). The clean data set with well-measured magnitudes from the software consists of 112 data points (Fig. 2). We then perform a period search using the Lomb-Scargle (Lomb 1976; Scargle 1982) periodogram. The periodogram is then normalized by the residuals of the data around a constant reference model. The periodogram (Fig. 3) clearly shows an isolated peak at a period of 1.96 days, the precision with which this peak’s frequency can be identified is directly related to the width of this peak. For the uncertainty in the period we take the σ of the Gaussian fit of

the peak ~ 0.06 day. We also calculate a false alarm probability of 6.6×10^{-32} using the method described in Baluev (2008). The folded lightcurve at that period is shown in Fig. 4.

We also perform a periodicity analysis using the phase dispersion minimization technique (PDM Stellingwerf 1978). In this method, the lightcurve is divided into different phase bins and the cost function, $\Theta = s^2/\sigma^2$, is minimized to choose the best period. Here s is the phase bin variance and σ is the total data variance. We divide the data into 10 equidistant bins to calculate Θ . The plot of the ratio Θ vs. period (inset in Fig. 3) is a good indicator for the best period. The local minimum corresponds to $\Theta = 0.1365$ at a period of 1.98 days, consistent with the results obtained with the Lomb-Scargle periodogram. To calculate the false alarm probability (FAP), an estimate of the significance of the minimum against the hypothesis of random noise, Schwarzenberg-Czerny (1997) showed that the PDM statistic follows a beta distribution and thus the FAP can be calculated as:

$$\text{FAP} = 1 - \left[1 - \beta \left(\frac{N-M}{2}, \frac{M-1}{2}, \frac{(N-M) \times \Theta}{N-1} \right) \right]^m$$

where N is the total number of data points, M is the number of bins, Θ is the value of the PDM theta statistic, and m is the effective number of independent frequencies. The number of independent frequencies can be estimated in a number of ways (e.g., Linnell Nemeč & Nemeč 1985; Horne & Baliunas 1986; Cumming 2004), here we follow the conservative prescription given in Schwarzenberg-Czerny (2003) and choose $m = \min(N, N_f, \Delta f \Delta T)$ where N_f is the number of frequencies, Δf is the frequency range and ΔT is the time span of observations. This gives a very small FAP of 5×10^{-40} .

Red noise can produce spurious detections of periodic behaviour in datasets with small numbers of cycles of the putative period (Press 1978). To test against this possibility, we simulate random red noise light curves following the algorithm detailed in Timmer & Koenig (1995). The algorithm randomizes the phases and the amplitudes of an underlying power law spectrum by drawing two sets of normally distributed numbers, and then inverse Fourier transforming them. First, we produce a simulated light curve that exhibits a power law spectrum of the form $(1/f)^2$ evenly sampled at the exposure time of our observations (~ 10 min). Then, we add random Gaussian noise with the same mean and variance as the errors from the observations. The next step is to re-sample the simulated light curve with noise added and re-scale it to have the same sampling characteristics, mean and variance as the light curve of the observation. For each generated mock light curve, we compare the maximum power in the Lomb-Scargle periodogram to that of the observed periodicity. We repeat this step 10^6 times to estimate the probability that the found periodicity is due to underlying red noise. In our 10^6 trials, only 10 periodograms had a higher power than the one found in the real lightcurve. This corresponds to a probability of 0.001%. In all cases, the spurious periods were 8-10 days, much longer than the real one. Our data spans a bit more than 13 period cycles, and fig. 3 clearly show only weak variability on longer timescales. In combination with the other indications that the system should have an orbital period of about 2 days, discussed below, the number of observed cycles and our simulated lightcurves present a strong case against a spurious period due to red noise.

3 RESULTS AND DISCUSSION

The strong optical modulations at 1.96 ± 0.06 days can be explained by the heating of one side of the companion by radiation from

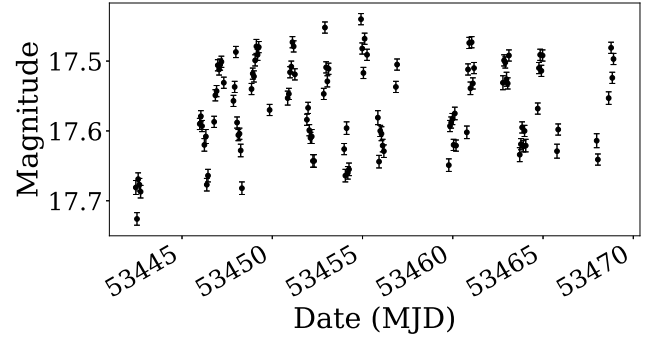


Figure 2. Lightcurve for the redback millisecond pulsar candidate, U18. The magnitudes are from the F336W filter without dereddening and magnitudes uncertainty from the DOLPHOT output catalog.

the pulsar, as seen in other confirmed redbacks in the field (e.g., Hui et al. 2015; Salvetti et al. 2015). This interpretation is further strengthened by the recently reported steep radio spectrum of U18 (Zhao et al. 2020). Zhao et al. (2020) report a spectral flux density at 5.5 GHz of $S_\nu = 54.7 \mu\text{Jy}$. A 1.96 day orbit would put U18 as the longest period confirmed redback in a globular cluster, and one of the few redbacks with an orbital period longer than 1 day in the Galactic field. Two other redbacks in the field, 1FGL J1417.7-4407 (Strader et al. 2015; Camilo et al. 2016; Swihart et al. 2018) and 2FGLJ0846.0+2820 (Swihart et al. 2017) have longer periods at 5.3 and 8.3 day respectively.

The strong radio emission also argues against an active binary scenario. Guedel & Benz (1993) found that for coronally active stars, typically $\log(L_R/L_X) \sim -15.5 \text{ Hz}^{-1}$. From this relationship, for U18, assuming a $L_X = 6.7 \times 10^{31} \text{ ergs s}^{-1}$ (0.3-8 keV) (Bogdanov et al. 2010), $L_R = 2 \times 10^{16} \text{ ergs s}^{-1} \text{ Hz}^{-1}$. This is an order of magnitude lower than the reported value for $L_R(5.5 \text{ GHz}) = 3.8 \times 10^{17} \text{ ergs s}^{-1} \text{ Hz}^{-1}$ reported by Zhao et al. (2020).

The optical to X-ray luminosity argues further against the active binary scenario. Pallanca et al. (2017) calculate the dereddened magnitude for U18 as $V_0 = 16.05$, from the HST F555W observations of the cluster. We take a distance modulus $(m-M)_0 = 12.01$ (Gratton et al. 2003) and a $T_{\text{eff}} = 4200 \text{ K}$ (Husser et al. 2016). We can use the Flower (1996) bolometric correction to find a bolometric luminosity, $L_{\text{opt}} = 1.6 \times 10^{34} \text{ ergs s}^{-1}$. Then, with $L_X = 6.7 \times 10^{31} \text{ ergs s}^{-1}$ (0.3-8 keV; Bogdanov et al. 2010), we determine that the ratio is $L_X/L_{\text{opt}} = 4.2 \times 10^{-3}$, well above the saturation limit of 10^{-3} for active binaries (Vilhu 1984; Vilhu & Walter 1987), arguing strongly against that scenario. We can further exclude the possibility that the X-rays were measured during a flaring event. Large flares, with total energies of order $10^{37} \text{ ergs s}^{-1}$ (0.1-2.4 keV) have been detected in active binary systems, like RS CVn (e.g., Kuerster & Schmitt 1996). U18 has been observed in five different epochs from 2000 to 2007 for a total of 340 ks in the X-ray with Chandra. Bogdanov et al. (2010) analyzed all 5 observations and reported similar count rates for all of them, making it less likely that U18 was caught during a flaring event. Additionally, using the same data sets than Bogdanov et al. (2010), we also searched for candidate periods in the archive Chandra X-ray data, but the sampling of the data is not ideal to find a period in the order of days, and we did not find any convincing periodicity in the X-rays (not even folding at the optical period we identified).

The radio emission also makes the identification as a CV less likely. Furthermore, Cohn et al. (2010) examined the ratio of X-

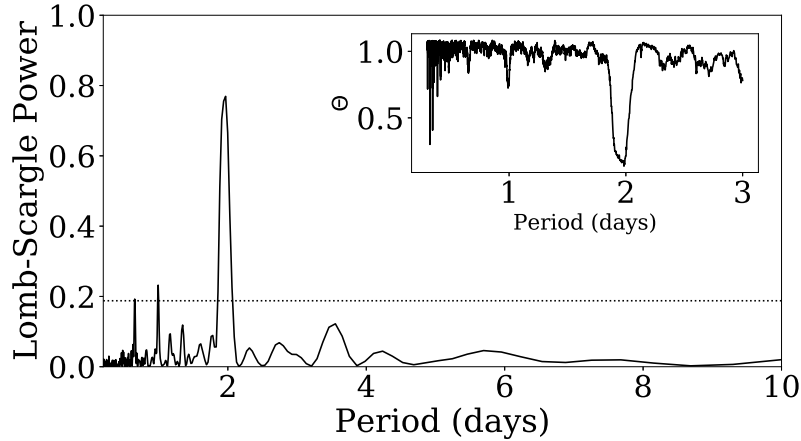


Figure 3. Lomb-Scargle Periodogram for U18, showing a clear isolated peak around 1.96 days. The dotted line shows the periodogram level corresponding to a maximum peak false alarm probability of 1%, using the bootstrap method that simulates data at the same observation times to approximate the true distribution of peak maxima for the case with no periodic signal present. The bootstrap method is performed with periods between 0.1 and 10 days, and after normalizing by the residuals of the data around a constant reference model. The inset on the graph shows the Θ statistics as defined by Stellingwerf (1978). The period that minimizes the dispersion of the data at constant phase is ~ 1.98 days.

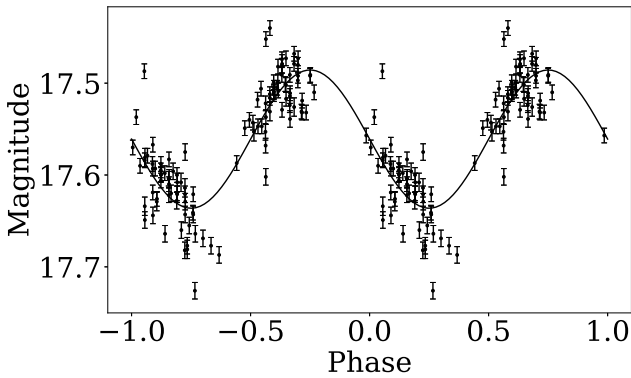


Figure 4. Lightcurve for U18 folded on the 1.96 day period. The magnitudes are from the F336W filter without dereddening.

ray to optical flux for many optical counterparts of Chandra X-ray sources. They conclude that U18 has a similar ratio to the confirmed MSP U12 and separated from other CV candidates. Also Pallanca et al. (2017) looked at the equivalent width of the $H\alpha$ emission of U18 and measured an equivalent width similar to U12 and smaller than other confirmed CV and CV candidates in the cluster. All this argues against U18 being a CV candidate.

We can use the proposed orbital period to find some constraints on the properties of U18. From the obtained orbital period and the X-ray luminosity, we can place a limit on the spin-down luminosity. We use the relation from Possenti et al. (2002)

$$L_x = 10^{-15.3} \times L_{sd}^{1.34}$$

where L_x is the X-ray luminosity from 2-10 KeV and L_{sd} is the spin-down luminosity. A $L_x = 6.7 \times 10^{31}$ ergs s^{-1} (0.3-8 keV; Bogdanov et al. 2010) gives a $L_{sd} = 1.47 \times 10^{35}$ ergs s^{-1} . Assuming that the system is close to being Roche-lobe filling and using the relationship from Eggleton (1983), for a mass range of $q \sim 0.1 - 1$, the companion would receive a total power output on the order of $\times 10^{33}$ ergs s^{-1} . This corresponds to $\sim 10\%$ of the total bolometric luminosity of the star. Relating this power to the Δmag observed for this system requires more data in other wavelengths to do an

accurate modelling taking into account the albedo and the fraction of light from intrabinary shocks in the system. Furthermore, the light curve is in F336W or near UV where in other systems it has been shown that there is variability due to intrabinary shocks (e.g. Rivera Sandoval et al. 2018). In other systems where no ellipsoidal variations are observed the magnitude of the modulations decreases toward longer wavelengths (e.g. Baglio et al. 2016). U18 is near the core of the cluster and only $\sim 0.2''$ from a brighter star. Due to extreme crowding at redder wavelengths and possibly lower amplitude of modulations, we limit the variability study to the F336W data. Future data with adaptive optics or speckle interferometry to study the variability of this source at redder bands would allow to do a detailed modeling of the system.

Other evidence that points to intrabinary shocks as the source of the blue light is the observed colors for U18. The V-I colors of this object, $V-I = 0.93$ (Pallanca et al. 2017), are significantly bluer than expected for a $T_{eff} = 4200$ K star (Pecaut & Mamajek 2013) (which is indicated from spectroscopy), indicating that there is an extra component providing blue continuum light. This means that the observed flux is a combination of emission from the companion star and from the intrabinary shock, making the companion to look brighter and 'bluer' than in reality.

We also compared the observed limits on the size of the donor star with predictions for nearly Roche-lobe filling companions at different orbital periods in order to test whether the 1.96 day period is the actual orbital period or a harmonic of the orbital period (as might be expected if the modulations are ellipsoidal). In redder bands we expect light to be dominated by the companion. For a star of $T_{eff} \approx 4200$ K, the theoretical radius is $R_{\odot} = 0.676R_{\odot}$ and the absolute magnitude in the I band $M_I = 6.2$ (Pecaut & Mamajek 2013). Using the extinction from Richer et al. (2008), this gives a theoretical magnitude in the I band of $M_I = 5.87$. We can compare this to the reported values in the I band for U18. From Pallanca et al. (2017) the absolute magnitude of U18 is $M_{I_o} = 3.210$, comparing these two values, we can infer that the companion is 11.5 times brighter than a theoretical star at the same T_{eff} , and thus has a radius $R \approx 2.3R_{\odot}$. Assuming typical values for the mass ratio $q = 0.16$ and the mass of the neutron star, $M_{NS} = 1.76$ (Strader et al. 2019). For the proposed orbital period of 1.96 days, assuming

a Roche-lobe filling companion, as is the case in many redbacks, and using the Paczyński (1971) relations for the radius of a Roche-lobe star and Kepler's second law we get an estimated radius of the companion of $R_{\text{companion}} = 2R_{\odot}$. This is close to the estimated value of the radius from the measured I band flux of U18. A longer orbital period of $P_{\text{orb}} = 2 \times 1.96$ days gives a $R_{\text{companion}} = 3.2R_{\odot}$. To get a $R_{\text{companion}} = 2R_{\odot}$ with twice the proposed orbital period, the mass ratio would need to be low compare to other known Redbacks (Strader et al. (2019) reports a minimum $q = 0.07$) and would make the companion a star with $M = 0.07M_{\odot}$ and $R = 2R_{\odot}$, making it a system with an unusually low mass ratio. All this argues for the period to be 1.96 days and argues against a longer orbital period.

4 ACKNOWLEDGEMENT

This research made use of Astropy (Astropy Collaboration et al. 2013; Price-Whelan et al. 2018) and Matplotlib (Hunter 2007).

5 DATA AVAILABILITY

This work used public data available in the Mikulski Archive for Space Telescopes under the programme GO-10424 (P.I.H.Richer).

REFERENCES

- Archibald A. M., et al., 2009, *Science*, 324, 1411
 Astropy Collaboration et al., 2013, *A&A*, 558, A33
 Bacon R., et al., 2014, *The Messenger*, 157, 13
 Baglio M. C., D'Avanzo P., Campana S., Coti Zelati F., Covino S., Russell D. M., 2016, *A&A*, 591, A101
 Baluev R. V., 2008, *MNRAS*, 385, 1279
 Bassa C. G., et al., 2014, *MNRAS*, 441, 1825
 Benvenuto O. G., De Vito M. A., Horvath J. E., 2014, *ApJ*, 786, L7
 Bogdanov S., Grindlay J. E., van den Berg M., 2005, *ApJ*, 630, 1029
 Bogdanov S., van den Berg M., Heinke C. O., Cohn H. N., Lugger P. M., Grindlay J. E., 2010, *ApJ*, 709, 241
 Bogdanov S., Archibald A. M., Hessels J. W. T., Kaspi V. M., Lorimer D., McLaughlin M. A., Ransom S. M., Stairs I. H., 2011, *ApJ*, 742, 97
 Callanan P. J., van Paradijs J., Rengelink R., 1995, *ApJ*, 439, 928
 Camilo F., et al., 2016, *ApJ*, 820, 6
 Chen H.-L., Chen X., Tauris T. M., Han Z., 2013, *ApJ*, 775, 27
 Cho P. B., Halpern J. P., Bogdanov S., 2018, *ApJ*, 866, 71
 Cohn H. N., et al., 2010, *ApJ*, 722, 20
 Cool A. M., Grindlay J. E., Krockenberger M., Bailyn C. D., 1993, *ApJ*, 410, L103
 Cool A. M., Grindlay J. E., Cohn H. N., Lugger P. M., Slavin S. D., 1995, *ApJ*, 439, 695
 Cool A. M., Grindlay J. E., Cohn H. N., Lugger P. M., Bailyn C. D., 1998, *ApJ*, 508, L75
 Cumming A., 2004, *MNRAS*, 354, 1165
 D'Amico N., Lyne A. G., Manchester R. N., Possenti A., Camilo F., 2001, *ApJ*, 548, L171
 Dieball A., Rasekh A., Knigge C., Shara M., Zurek D., 2017, *MNRAS*, 469, 267
 Dolphin A. E., 2000, *PASP*, 112, 1383
 Eggleton P. P., 1983, *ApJ*, 268, 368
 Ferraro F. R., Possenti A., D'Amico N., Sabbi E., 2001, *ApJ*, 561, L93
 Flower P. J., 1996, *ApJ*, 469, 355
 Fruchter A. S., Stinebring D. R., Taylor J. H., 1988a, *Nature*, 333, 237
 Fruchter A. S., Gunn J. E., Lauer T. R., Dressler A., 1988b, *Nature*, 334, 686
 Gratton R. G., Bragaglia A., Carretta E., Clementini G., Desidera S., Grindlay J. E., Lucatello S., 2003, *A&A*, 408, 529
 Grindlay J. E., Cool A. M., Callanan P. J., Bailyn C. D., Cohn H. N., Lugger P. M., 1995, *ApJ*, 455, L47
 Grindlay J. E., Heinke C. O., Edmonds P. D., Murray S. S., Cool A. M., 2001, *ApJ*, 563, L53
 Guedel M., Benz A. O., 1993, *ApJ*, 405, L63
 Harris W. E., 1996, *AJ*, 112, 1487
 Heinke C. O., et al., 2014, *MNRAS*, 444, 443
 Horne J. H., Baliunas S. L., 1986, *ApJ*, 302, 757
 Hui C. Y., et al., 2015, *ApJ*, 801, L27
 Hunter J. D., 2007, *Computing in Science & Engineering*, 9, 90
 Husser T.-O., et al., 2016, *A&A*, 588, A148
 Kaluzny J., Thompson I. B., Krzeminski W., Schwarzenberg-Czerny A., 2006, *MNRAS*, 365, 548
 Kandel D., Romani R. W., 2020, *ApJ*, 892, 101
 Kuerster M., Schmitt J. H. M. M., 1996, *A&A*, 311, 211
 Linares M., 2018, *MNRAS*, 473, L50
 Linnell Nemec A. F., Nemec J. M., 1985, *AJ*, 90, 2317
 Lomb N. R., 1976, *Ap&SS*, 39, 447
 McLaughlin D. E., van der Marel R. P., 2005, *ApJS*, 161, 304
 Paczyński B., 1971, *ARA&A*, 9, 183
 Pallanca C., Beccari G., Ferraro F. R., Pasquini L., Lanzoni B., Mucciarelli A., 2017, *ApJ*, 845, 4
 Papatito A., et al., 2013, *Nature*, 501, 517
 Pecaum J., Mamajek E. E., 2013, *ApJS*, 208, 9
 Possenti A., Cerutti R., Colpi M., Mereghetti S., 2002, *A&A*, 387, 993
 Press W. H., 1978, *Comments on Astrophysics*, 7, 103
 Price-Whelan A. M., et al., 2018, *AJ*, 156, 123
 Richer H. B., et al., 2006, *Science*, 313, 936
 Richer H. B., et al., 2008, *AJ*, 135, 2141
 Rivera Sandoval L. E., et al., 2018, *MNRAS*, 475, 4841
 Roberts M. S. E., 2013, in van Leeuwen J., ed., *IAU Symposium Vol. 291, Neutron Stars and Pulsars: Challenges and Opportunities after 80 years*, pp 127–132 (arXiv: 1210.6903), doi:10.1017/S174392131202337X
 Romani R. W., Sanchez N., 2016, *ApJ*, 828, 7
 Salvetti D., et al., 2015, *ApJ*, 814, 88
 Scargle J. D., 1982, *ApJ*, 263, 835
 Schwarzenberg-Czerny A., 1997, *ApJ*, 489, 941
 Schwarzenberg-Czerny A., 2003, in Sterken C., ed., *Astronomical Society of the Pacific Conference Series Vol. 292, Interplay of Periodic, Cyclic and Stochastic Variability in Selected Areas of the H-R Diagram*, p. 383
 Shara M. M., Hinkley S., Zurek D. R., Knigge C., Dieball A., 2005, *AJ*, 130, 1829
 Stappers B. W., Gaensler B. M., Kaspi V. M., van der Klis M., Lewin W. H. G., 2003, *Science*, 299, 1372
 Stellingwerf R. F., 1978, *ApJ*, 224, 953
 Strader J., et al., 2015, *ApJ*, 804, L12
 Strader J., et al., 2019, *ApJ*, 872, 42
 Swihart S. J., et al., 2017, *ApJ*, 851, 31
 Swihart S. J., et al., 2018, *ApJ*, 866, 83
 Swihart S. J., et al., 2020, *ApJ*, 892, 21
 Taylor J. M., Grindlay J. E., Edmonds P. D., Cool A. M., 2001, *ApJ*, 553, L169
 Thorstensen J. R., Armstrong E., 2005, *AJ*, 130, 759
 Timmer J., Koenig M., 1995, *A&A*, 300, 707
 Vilhu O., 1984, *A&A*, 133, 117
 Vilhu O., Walter F. M., 1987, *ApJ*, 321, 958
 Zavlin V. E., Pavlov G. G., Shibanov Y. A., 1996, *A&A*, 315, 141
 Zavlin V. E., Pavlov G. G., Sanwal D., Manchester R. N., Trümper J., Halpern J. P., Becker W., 2002, *ApJ*, 569, 894
 Zhao Y., et al., 2020, *MNRAS*, 493, 6033

This paper has been typeset from a \LaTeX file prepared by the author.